

Local indices for the South American monsoon system and its impacts on Southeast Brazilian precipitation patterns

David Marcolino Nielsen¹ · Marcio Cataldi¹ · André Luiz Belém¹ · Ana Luiza Spadano Albuquerque²

Received: 13 January 2016 / Accepted: 9 May 2016 / Published online: 19 May 2016
© Springer Science+Business Media Dordrecht 2016

Abstract The South American monsoon system (SAMS) plays a fundamental role in the precipitation regime of the most populous and economically important regions in Brazil. The South Atlantic Convergence Zone (SACZ) is a main component of the SAMS, characterizing its active phase, and is often associated with intense rainfall events: Strong and persistent episodes cause severe floods and landslides, while weak and sparse episodes are associated with droughts. The variability of the convergence zone caused great natural disasters in Southeast Brazil, associated with extreme precipitation conditions: 3562 landslides killed 947 people in Rio de Janeiro state in 2011, while a shortage of water in São Paulo affected around 20 million people between 2014 and 2015. In the present study, we build SACZ configuration series for the period between January 2000 and June 2014 and use them as indicators for the SAMS to quantify its influence on several atmospheric variables. Based on a principal component analysis, we present indices that identify the configuration of the SACZ in a local scale. The indices reached strong accuracy rates, especially for identifying days of extreme rainfall events associated with the SAMS and may, thus, serve as decision-making tools to help prepare for their impacts. Furthermore, the indices are composed by common variables simulated by numerical weather and climate models, other than precipitation, which is often a not very reliable output. The applied methodology is easily reproducible and different variables may be used to compose indices for different regions—an advantage of this local-scale approach.

Keywords SAMS · SACZ · South Atlantic Convergence Zone · Intense rainfall · Monsoon index

✉ David Marcolino Nielsen
davidnielsen@id.uff.br

¹ Departamento de Engenharia Agrícola e do Meio Ambiente, Universidade Federal Fluminense, Rua Passo da Pátria, 156 bl D sl 236, São Domingos, Campus Praia Vermelha, Niterói, RJ CEP: 24210-240, Brazil

² Departamento de Geoquímica, Universidade Federal Fluminense, Outeiro São João Baptista, s/n, Niterói, RJ CEP: 24020-150, Brazil

1 Introduction

Increasing attention has been given to climate variability due to its impacts on society. Several studies have demonstrated the influence of water availability on aspects related to health, habitation and safety (Ahern et al. 2005; Siegel 2014; Spokane et al. 2013; Güneralp et al. 2015) and the relationship between precipitation and vegetation growth in South America, specifically (Barbosa et al. 2015). Numerical modeling is frequently applied to assess the risk of adverse weather conditions, such as floods and droughts (Milly et al. 2002; Murphy et al. 2001). Therefore, an accurate understanding of the components of the climate system variability modes is crucial to assemble decision-making tools, allowing a better control over the impacts of natural disasters on determined regions.

Major floods are responsible for deaths and severe economic impacts, which are often related to the dynamics of monsoon systems (Singh and Kumar 2013). The South American monsoon system (SAMS) is one of the most important phenomena related to intense precipitation during the wet season of the most populous and economically important regions of Brazil, being associated with the typical austral-summer warming pattern, which originates the South Atlantic Convergence Zone (SACZ) (Vera et al. 2006a). Summed to certain conditions of other dynamic-atmospheric and oceanic systems, such as the positioning of the South Atlantic Subtropical Anticyclone (SASA), sea surface temperature (SST) variations and the periodicity of cold fronts, the SAMS is therefore also responsible for modulating the climate over these regions, with direct impacts on the seasonal precipitation regime (Minuzzi et al. 2007).

Strong and persistent SACZ conditions are often associated with intense rainfall events, causing severe floods and landslides (Seluchi and Chou 2009). During the austral summers of 2010/2011 and 2012/2013, SACZ configurations were directly responsible for hundreds of deaths and thousands of homeless in Rio de Janeiro state (Saraiva et al. 2015). One single episode of the convergence zone caused 3562 landslides in the mountainous region of Rio de Janeiro (Avelar et al. 2013) and 947 human losses between January 11 and 12, 2011 (Dourado et al. 2012), cited as “one of the worst natural disasters in Brazil’s history” by the World Meteorological Organization (WMO 2012). Figure 1a illustrates some of the

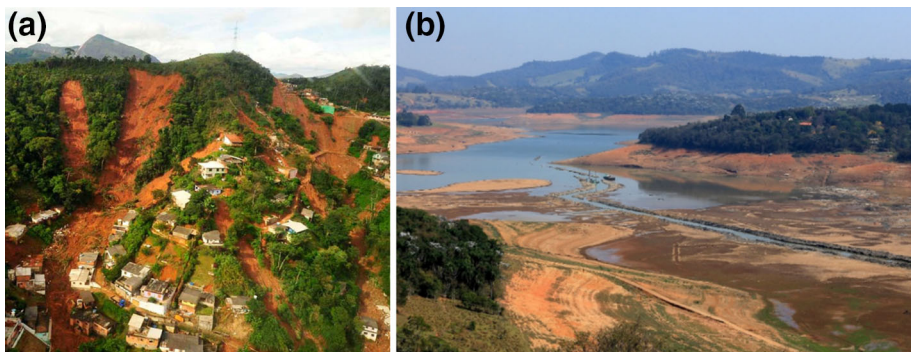


Fig. 1 **a** Landslides in Nova Friburgo, mountainous region of Rio de Janeiro, during the SACZ episode occurred between the January 11 and 12, 2011 (G1 News Agency, from <http://g1.globo.com/rio-de-janeiro/noticia/2011/01/regiao-serrana-do-rj-enfrenta-2-dia-de-calamidade-causada-pela-chuva.html>). **b** A view of the dry Jacareí river dam, part of the Cantareira reservoir system in São Paulo, in September 2014 (Uol News Agency, from <http://noticias.uol.com.br/album/album-do-dia/2014/09/16/imagens-do-dia—16-de-setembro-de-2014.htm#fotoNav=26>)

landslides occurred during this SACZ episode: In 2 days, the accumulated volume of rainfall reached 166 mm in Nova Friburgo (Rio de Janeiro), which is 70 % of climatological mean for the entire month of January (237.4 mm) (Climanálise 2011). According to Lima et al. (2010), almost all natural disasters in Southeast Brazil are caused by heavy rainfall events: 53 % of these are due to cold front passages, while the remaining 47 % are related to the SACZ. Carvalho et al. (2002) also demonstrated that extreme precipitation events in São Paulo, specifically, are associated with the SACZ, mainly during its intense and extensive episodes over the adjacent Atlantic Ocean. Figure 2 displays the Southeast Brazilian region containing the locations cited in this work.

On the other hand, extremely dry conditions in Southeast Brazil are associated with less frequent or weak episodes of the SACZ during the SAMS active period, such as during the 2001 austral summer (Drumond and Ambrizzi 2005) and more recently between 2013 and 2015 (Coelho et al. 2015b). In both of these situations, the Brazilian national interconnected power generation system, which is 77 % dependent on hydraulic generation (based on data from 2013, ONS), was compromised, due to the most important reservoirs being in the area where precipitation volumes are directly influenced by the convergence zone. The SACZ is also a main factor to determine the levels of the water supply systems for human consumption of the most densely populated regions of Brazil. Around 20 million people were affected by water rationing programs in São Paulo during the austral summers of 2013/2014 and 2014/2015. In January 2015, the reservoirs of Cantareira system, the biggest in São Paulo, reached less than 5 % of its storage capacity, due to the reduced number of SACZ episodes (Coelho et al. 2015a), as illustrated in Fig. 1b.

According to Quadro (1999), the SACZ is identified as a band of deep clouds oriented in the NW–SE direction, extending from the Amazonian region to central South Atlantic Ocean. When active, the SACZ shows several identifying characteristics in both high and low atmospheric levels. The flow in around 200 hPa presents the Bolivian High (BH), a quasi-stationary anticyclone system extending over most of South America north of 35°S, as early described by Prohaska (1976), and the a upper-troposphere cyclonic vortex over the Northeast of Brazil to the east of the BH—the “Nordeste low,” whose formation is dynamically linked to the presence of the BH, to the penetration cold frontal systems (Kousky and Gan 1981) and to the convection associated with summertime heating in the

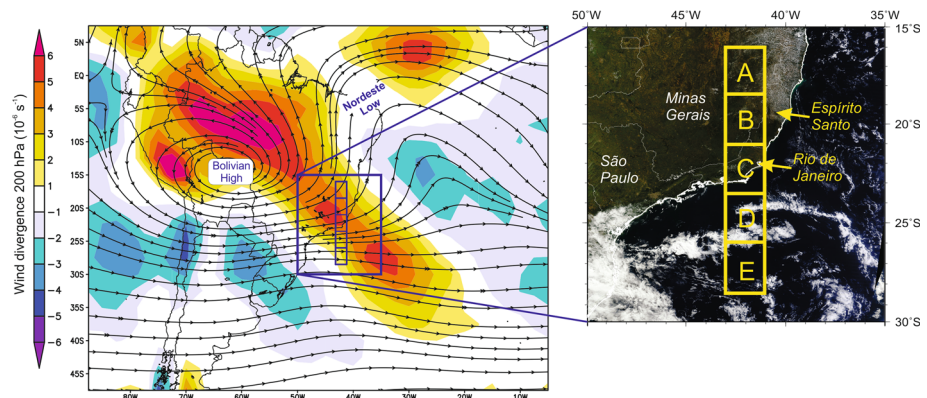


Fig. 2 Wind streamlines and horizontal divergence at 200 hPa averaged during all days with SACZ episodes between January 2000 and April 2014 (left) and a highlight of the study areas within the Southeast region of Brazil (right)

Amazonian region (Silva Dias et al. 1983). The Nordeste low is also maintained by a direct thermal circulation, with cold subsidence in its center and warm air rising in its periphery (Kousky and Gan 1981). Lenters and Cook (1997) simulated the atmospheric dynamics of South America with and without its topography and showed that the BH is associated mainly with summertime condensational heating, as a response to precipitation in the Amazon, central Andes and the SACZ region. The Andean mountains would have an indirect influence on the upper-level circulation, helping modulate precipitation in central Andes and the SACZ. Figure 2 presents the circulation at 200 hPa averaged during all days with SACZ episodes between January 2000 and the end of the 2014 summer (averages are further discussed in the methodology section), where the typical configuration of the BH is shown and the Nordeste low figures as an open trough system.

Closer to the surface, moisture convergence occurs in the NW–SE direction, maintaining a continuous water vapor flux and an equivalent potential temperature gradient, which determines the mean separating region defined between the warm and wet air mass, coming from the tropics, and the colder and dry mass, from higher latitudes (Ferreira et al. 2004). A consequence to the surface convergence is seen in high atmospheric levels, where a diagonal mean region of horizontal wind divergence occurs, as shown in Fig. 2.

Besides these simultaneous conditions, the cloud band should persist for at least 4 days for a SACZ to be classified. For its maintenance, it is essential that the moisture transport, carried by the east-of-Andes low-level jet (LLJ), from the Amazonian basin to higher latitudes, is displaced pointing to the Southern Atlantic Ocean (Ferreira et al. 2004). The LLJ is a zone of maximum winds flowing in the first kilometers of the atmosphere, typically between 600 and 900 hPa, presenting sub-synoptic dimensions (Bluestein 1992). It shows a significant diurnal cycle (Nicolini et al. 2004) and plays an important role in the low-level circulation, transporting heat and moisture from tropics toward the poles (Stensrud 1996), until the central and subtropical South America, with a maximum wind speed of about 25 m s^{-1} at 700–800 hPa (Vera et al. 2006b). Van der Ent et al. (2010) suggest that 70 % of the water in Río de la Plata basin (subtropical South America) depends on Amazonian evaporation.

Among the meteorological systems that support the SACZ, the SAMS and the LLJ have suffered significant variations with time and are still susceptible to changes related to anthropic influence. The transport of moisture performed by the LLJ depends on its availability in the Amazonian region and its capacity to store it during springtime (Contador et al. 2013). Lejeune et al. (2015) have shown that deforestation of the Amazonian forest should be followed by a decrease in precipitation, which may, thus, have an impact on the amount of moisture carried by the LLJ to higher latitudes and, consequently, on the SAMS regime. These changes, therefore, may be associated with precipitation anomalies observed in Southeast Brazil (Zilli and Carvalho 2013).

Being able to quantify the frequency and intensity of precipitation anomalies associated with the SAMS is a key to better understand its natural variability, providing support for predicting extreme hazardous conditions (dry and wet) and mitigating its negative consequences. Traditionally, outgoing longwave radiation (OLR) anomalies have been used to identify and classify the SACZ (e.g., Kousky 1988; Carvalho et al. 2002; Andrade and Marton 2008). Jones and Carvalho (2001) also investigated patterns of low-level wind anomalies associated with the SAMS cycle. More recently, Ambrizzi and Ferraz (2015) proposed a criterion based on observational precipitation data to determine the SACZ configuration. However, Gan et al. (2005) already showed that low-level circulation should be considered to compose SAMS indices and that numerical models have more skill predicting wind than precipitation in certain regions of Brazil. Silva and Carvalho (2007)

suggested an index to represent large-scale features of the SAMS, also including precipitation data in its composition.

In the present study, we aim to develop indices that take into account the complexity of the SAMS and its main components in their three-dimensional, but local scale. Once the active phase of the SAMS is characterized by the presence of the SACZ configurations, representing its subtropical portion (Carvalho et al. 2011), the SACZ is used as an indicator for the monsoon system and its impacts on several atmospheric variables are assessed, other than OLR and precipitation only. Therefore, the presented indices correlate with precipitation anomalies associated with the convergence zone, which is a local consequence of the monsoon system, instead of an explanatory variable. We also choose not to use precipitation to compose the indices due to this variable's outputs from numerical models being not as reliable as other atmospheric fields, used to compose our indices, as pointed by Gan et al. (2005). In addition, the present indices have solely a local character and only take into account the effects of the SAMS in specific regions in Southeast Brazil. By identifying the effects of SACZ episodes, we hope to provide support for its assessment through past time and better understand its natural variability. In addition, the local-scale indices may serve as decision-making tools, helping forecast hazardous conditions of intense rainfall episodes and prepare for their impacts.

2 Methodology

2.1 Study areas

Five areas were defined to quantify the influence of the SAMS on atmospheric variables. Each area (A, B, C, D, E) is 2° longitude wide, between 41°W and 43°W, and 2.5° latitude long, contained between 16°S and 28.5°S. The areas were determined considering the main position of the SACZ, as identified by Carvalho et al. (2002, 2004) via the study of OLR anomalies and by Mendonça and Bonatti (2008), through the assessment of the confluence of winds at 850 hPa. The study areas are located in Southeast Brazil, and their extension comprehends the latitudinal variation of the SACZ episodes during the considered period of this study (January 2000–June 2014). Figure 2 shows the location of the study areas in comparison with the composite main circulation at 200 hPa and horizontal wind divergence averaged during the days in which the SACZ occurred in this period (left) and within the Southeast region of Brazil (right).

2.2 Datasets

Daily series of specific humidity at 2 m above the surface, OLR, cloud cover, surface air temperature, zonal and meridional components of wind (u and v), vertical velocity (dp/dt , ω), horizontal wind divergence and vorticity at 500, 850 and 1000 hPa were obtained from Reanalysis 2 project from the National Center for Environment Predictions (NCEP/NCAR) (Kalnay et al. 1996). Averaged daily and pentad anomalies were calculated (subtracted from long-term monthly means) over the study areas from January 2000 to June 2014, based on the climate obtained for this same period. Aiming to assess the impact of the SACZ on these local climate variables, daily SACZ Boolean series (1 for present or 0 for absent) were built for each study area, after the analysis of Climanálise Bulletin (Climanálise Boletim), published by the Brazilian Center of Weather Forecast and Climate Studies (*Centro de Previsão do Tempo e Estudos Climáticos*—CPTEC/INPE). For these

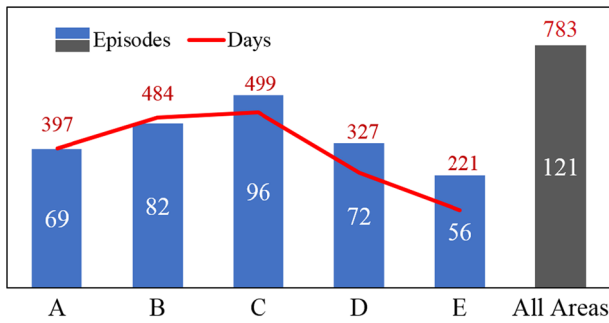


Fig. 3 Histogram of distribution of SACZ episodes (blue and gray bars) and days with SACZ episodes (red numbers) per study area

series, episodes of moisture convergence zone (MCZ) were also considered due to their physical processes being similar to the SACZ, as first described by Neto et al. (2010), and in order to improve the statistical significance of the present analysis. For sake of simplicity, the MCZ will hereafter be referred to as SACZ as well. From January 2010 until the end of the 2014 summer, 121 episodes of SACZ were identified in all regions, spatially spreading in 69, 82, 96, 72 and 56 episodes in regions A, B, C, D and E, respectively, as shown in Fig. 3. The distribution of (days with) SACZ episodes per study area resembles a normal distribution, however asymmetric, with the maximum frequency centered in the middle area C.

2.3 Identifying the influence of the SACZ on atmospheric variables

A sequence of analysis of conditional probabilities was performed to identify and measure the influence of the convergence zone episodes on the selected variables in a local scale. Initially, all the daily series of anomalies of the atmospheric variables were averaged in pentads, as well as the daily series of occurrences of the SACZ. For the latter, a pentad in which the convergence zone was configured in 1–5 days, was considered a “SACZ-pentad.” Therefore, “non-SACZ pentads” only happened if the convergence zone did not occur in none of the 5 days. The probabilities of simultaneous configuration of the SACZ with positive and negative signals of the climate variables were calculated, for each study area, as shown in Table 1. The percentages are calculated given the number of pentads in which the SACZ occurred in each study area. Emphasized variables show at least a 30–70 % difference between these probabilities, suggesting a predominant anomalous signal of the atmospheric variables in pentads with episodes of the convergence zone.

The SACZ occurred predominantly in pentads with simultaneous positive anomalies of cloud covers in all areas, but with a stronger signal in the northernmost areas, as shown in Table 1. Predominant negative anomalies of OLR are also associated with the SACZ in the continental and northernmost areas A, B and C. This observed spatial gradient is explained due to the southernmost areas being more influenced by frequent cold fronts, which do not reach the northern regions so often and have similar effects on cloud cover and OLR in comparison with the SACZ, which influenced the regional long-term averages. Predominant positive anomalies of the zonal component of wind in low and medium atmospheric levels were also observed during SACZ-weeks, which relate to the diagonal NW–SE characteristic circulation of the SACZ, thus the eastward flow of moisture onto the study

Table 1 Probabilities of positive and negative anomalies of the considered atmospheric variables in pentads given the presence of the SACZ

Number of pentads with presence of the SACZ per study area	136		174		181		129		95	
	A		B		C		D		E	
	Anom +	Anom -								
Specific humidity at 2m	79%	21%	68%	32%	57%	43%	60%	40%	61%	39%
OLR	19%	81%	26%	74%	29%	71%	50%	50%	55%	45%
Surface air temperature	35%	65%	36%	64%	43%	57%	36%	15%	55%	45%
Zonal wind (u) at 500hPa	76%	24%	71%	29%	64%	36%	60%	40%	54%	46%
Zonal wind (u) at 850hPa	65%	35%	64%	36%	58%	42%	50%	50%	56%	44%
Zonal wind (u) at 1000hPa	68%	32%	62%	38%	58%	42%	52%	48%	57%	43%
Meridional wind (v) at 500 hPa	38%	62%	44%	56%	34%	66%	28%	72%	28%	72%
Meridional wind (v) at 850 hPa	38%	62%	47%	53%	46%	54%	43%	57%	45%	55%
Meridional wind (v) at 1000 hPa	42%	58%	46%	54%	53%	47%	51%	49%	48%	52%
Cloud cover	85%	15%	78%	22%	71%	29%	71%	29%	66%	34%
Omega at 500hPa	24%	76%	32%	68%	29%	71%	30%	70%	25%	75%
Omega at 850hPa	38%	62%	38%	62%	35%	65%	37%	63%	33%	67%
Omega at 1000hPa	58%	42%	52%	48%	43%	57%	41%	59%	36%	64%
Vorticity at 500 hPa	46%	54%	43%	57%	47%	53%	51%	49%	51%	49%
Vorticity at 850 hPa	43%	57%	41%	59%	40%	60%	42%	58%	41%	59%
Vorticity at 1000 hPa	35%	65%	38%	62%	38%	62%	33%	67%	34%	66%
Horizontal divergent at 500 hPa	60%	40%	48%	52%	46%	54%	41%	59%	41%	59%
Horizontal divergent at 850 hPa	29%	71%	30%	70%	39%	61%	40%	60%	31%	69%
Horizontal divergent at 1000 hPa	32%	68%	36%	64%	36%	64%	31%	69%	29%	71%

The percentages are calculated given the number of pentads in which the SACZ occurred in each study area

areas. Predominant negative anomalies of omega (vertical velocity) and the horizontal divergent of wind are also observed in pentads with the presence of the convergence zone, as expected. In regions A and B, a stronger signal of positive anomalies of close-to-surface specific humidity is noticed, which may be associated with increased precipitation as a consequence of the SACZ. Meanwhile, this is not so remarkable in regions that extend over the Atlantic Ocean (C, D and E), when the absence of clouds intensifies evaporation and consequently increases specific humidity as well, still during a typical no-SACZ condition.

This first assessment was rebuilt with a daily discretization, as shown in Table 2. This finer-precision analysis reinforced previous results, showing even stronger and more homogeneous differences in probabilities of anomalous signals of variables in days with SACZ episodes throughout the study areas. Up to 95 % of the 397 days with the presence of the convergence zone presented positive anomalies of cloud cover percentage in study area A, for example, as well as 93, 85 and 86 % presented negative anomalies of OLR, omega at 500 hPa and positive anomalies of the zonal component of wind at 500 hPa, respectively. In this second analysis, positive anomalies of the zonal component of wind characterize the NW–SE circulation of the SACZ, which was observed to be stronger in medium atmospheric levels (500 hPa) than in lower levels (850 and 1000 hPa), which may be explained by the influence of topography and near-surface dynamics on disturbing the atmospheric flow, as already noticed with the pentad analysis.

In a third analysis, the probabilities of positive and negative anomalous signals of the variables were again calculated, but out of a smaller set of days, where two conditions were imposed: simultaneous (1) configurations of the SACZ and (2) the anomalous value of the atmospheric variables being in the 40 % extremes (positive and negative) derived from their permanence curves. In other words, SACZ days where the atmospheric variables oscillated in the 60 % closer-to-the-average band were not taken into account. The first two columns of Table 3, for each study area, show the probabilities of occurrence of extreme

Table 2 Probabilities of positive and negative anomalies of atmospheric variables, given the number of days with the presence of the SACZ per study area

Number of days of episodes of SACZ per study area	397		484		499		327		221	
	A		B		C		D		E	
	Anom +	Anom -								
Specific humidity at 2m	85%	15%	73%	27%	57%	43%	64%	36%	69%	31%
OLR	7%	93%	13%	87%	15%	85%	17%	83%	19%	81%
Surface air temperature	31%	69%	32%	68%	35%	65%	47%	53%	56%	44%
Zonal wind (u) at 500hPa	86%	14%	82%	18%	73%	27%	54%	46%	55%	45%
Zonal wind (u) at 850hPa	71%	29%	63%	37%	55%	45%	55%	45%	52%	48%
Zonal wind (u) at 1000hPa	74%	26%	67%	33%	60%	40%	60%	40%	53%	47%
Meridional wind (v) at 500 hPa	38%	62%	37%	63%	31%	69%	25%	75%	19%	81%
Meridional wind (v) at 850 hPa	35%	65%	43%	57%	45%	55%	41%	59%	34%	66%
Meridional wind (v) at 1000 hPa	40%	60%	48%	52%	52%	48%	49%	51%	45%	55%
Cloud cover	95%	5%	93%	7%	90%	10%	88%	12%	86%	14%
Omega at 500hPa	15%	85%	19%	81%	19%	81%	19%	81%	19%	81%
Omega at 850hPa	37%	63%	31%	69%	26%	74%	23%	77%	20%	80%
Omega at 1000hPa	56%	44%	43%	57%	38%	62%	41%	59%	35%	65%
Vorticity at 500 hPa	48%	52%	40%	60%	42%	58%	44%	56%	45%	55%
Vorticity at 850 hPa	32%	68%	39%	61%	34%	66%	62%	38%	71%	29%
Vorticity at 1000 hPa	30%	70%	36%	64%	37%	63%	26%	74%	27%	73%
Horizontal divergent at 500 hPa	59%	41%	50%	50%	45%	55%	35%	65%	35%	65%
Horizontal divergent at 850 hPa	19%	81%	25%	75%	31%	69%	34%	66%	25%	75%
Horizontal divergent at 1000 hPa	28%	72%	25%	75%	26%	74%	23%	77%	20%	80%

positive and negative anomalies, given the number of days when the SACZ was present and the variables were in their extremes, simultaneously: $P(\text{anomalous signal} \mid \text{SACZ episode} \cap \text{extreme anomaly})$. The third column in Table 3 shows the number of days when this intersection occurred, given the total number of days with SACZ episodes, for each study area: $P(\text{SACZ episode} \cap \text{extreme anomaly} \mid \text{SACZ episodes})$. In region A, extreme anomalies of OLR were observed in 72 % of all days with SACZ episodes, and virtually 100 % of these anomalies were negative, for example.

In nearly 100 % of all days where the convergence zone occurred and the cloud cover percentage showed an extreme anomaly, this signal was positive in all study areas, except for region E, where 2 % of the days of extreme negative anomalies of cloud cover occurred together with the SACZ. A similar behavior is observed with OLR. Considering cloud cover and OLR as identifiers of the SACZ, their expected-signal probabilities being different from 100 % (given the presence of extreme positive OLR anomalies in SACZ days) may be explained by abrupt intra-day variations. For example, the convergence zone may establish itself, or move onto a certain area, in the evening of a day with predominantly clear-sky conditions (high OLR values), which is still considered an SACZ-day, however, with a counterintuitive extreme anomalous signal.

Quantifying the signature of the SACZ over the selected variables, by determining their predominant anomalous signal associated with the configuration of the convergence zone, made it possible to identify variables where this influence is clear. These variables are hereafter referred to as *signature variables* of the SACZ, and their predominant anomalous signals, associated with it, are referred to as its signature anomalous signals. Other two probability questions were formulated, in order to assess the possibility to determine the configuration of the convergence zone through considering these signature variables only: (a) What is the probability of having two variables showing the signature anomalous signal

Table 3 Probabilities of extreme positive and negative anomalies of the considered atmospheric variables, given the days when these anomalies were in their 40 % extremes simultaneously with SACZ episodes, and the percentages of days when this intersection (extreme anomaly \cap SACZ episode) occurred, given the total number of SACZ episodes, per study area

	A			B			C			D			E		
	+	-	%	+	-	%	+	-	%	+	-	%	+	-	%
Specific humidity at 2m	95%	5%	55	89%	11%	40	61%	39%	37	52%	48%	26	67%	33%	21
OLR	1%	99%	72	4%	96%	67	3%	97%	54	1%	99%	62	1%	99%	60
Surface air temperature	19%	81%	42	20%	80%	39	20%	80%	31	30%	70%	25	55%	45%	28
Zonal wind (u) at 500hPa	99%	1%	41	94%	6%	38	86%	14%	32	62%	38%	36	55%	45%	24
Zonal wind (u) at 850hPa	83%	17%	56	76%	24%	49	61%	39%	39	55%	45%	37	51%	49%	38
Zonal wind (u) at 1000hPa	87%	13%	54	77%	23%	48	67%	33%	39	61%	39%	35	46%	54%	36
Meridional wind (v) 500hPa	25%	75%	35	21%	79%	32	13%	87%	35	15%	85%	43	7%	93%	47
Meridional wind (v) 850hPa	29%	71%	48	37%	63%	46	46%	54%	45	39%	61%	46	30%	70%	42
Meridional wind (v) 1000hPa	38%	62%	52	52%	48%	48	63%	37%	41	64%	36%	35	42%	58%	38
Cloud cover	99%	1%	48	99%	1%	47	99%	1%	43	99%	1%	48	98%	2%	54
Omega at 500hPa	5%	95%	63	6%	94%	62	7%	93%	57	6%	94%	57	3%	97%	52
Omega at 850hPa	18%	82%	53	13%	87%	53	10%	90%	46	8%	92%	47	6%	94%	45
Omega at 1000hPa	60%	40%	48	41%	59%	48	31%	69%	46	36%	64%	49	26%	74%	48
Vorticity at 500 hPa	41%	59%	31	39%	61%	29	34%	66%	32	33%	67%	31	43%	57%	37
Vorticity at 850 hPa	23%	77%	58	4%	96%	64	22%	78%	52	13%	87%	45	20%	80%	37
Vorticity at 1000 hPa	26%	74%	50	29%	71%	46	28%	72%	39	17%	83%	44	10%	90%	42
Horizontal divergent 500hPa	67%	33%	49	50%	50%	43	43%	57%	44	32%	68%	43	38%	62%	44
Horizontal divergente 850hPa	8%	92%	56	13%	87%	51	25%	75%	45	22%	78%	46	12%	88%	46
Horizontal divergent 1000hPa	10%	90%	52	9%	91%	50	10%	90%	43	6%	94%	43	3%	97%	41

Emphasized values show greater differences between signals

simultaneously with episodes of SACZ, given the entire set of episodes of SACZ? and (b) What is the probability of having a SACZ episode simultaneously with two variables showing their signature anomalous signals, given the entire set of days in which this intersection occurs? In other words, questions *a* and *b* can be expressed as $P_a(x \cap y | ZCAS)$ and $P_b(ZCAS | x \cap y)$, respectively, where *x* and *y* represent the sets of days in which two variables presented their predominant anomalous signal associated with the SACZ (signature). Question *b*, therefore, addresses the possibility of identifying the SACZ by only considering the signature variables and their signature anomalous signal. Figure 4 illustrates questions *a* and *b* in Venn diagrams, where the highlighted gray areas and red circles represent the nominator and denominators of the probabilities' ratios, respectively. The answers for these questions are shown in Table 4.

The chance of having a day with the combination: negative anomaly of OLR and positive anomaly of cloud-cover percentage in days with episodes of the SACZ (question *a*) is

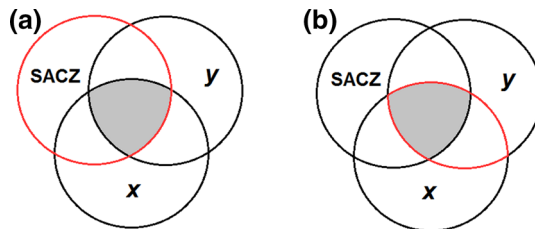


Fig. 4 Venn diagrams representing **a** $P_a(x \cap y | SACZ)$ and **b** $P_b(SACZ | x \cap y)$, where *x* and *y* represent the numbers of days in which two variables presented their predominant anomalous signal associated with the SACZ (signature). The highlighted gray areas and red circles represent the nominators and denominators of the probabilities' ratios, respectively

Table 4 Conditional probabilities combining pairs of variables: (a) $P_a(x \cap y | SACZ)$ and (b) $P_b(SACZ | x \cap y)$, where x and y represent the numbers of days in which two variables presented their signature anomalous signal (in parenthesis) for each study area

x	y	A		B		C		D		E	
		a (%)	b (%)								
OLR (-)	Cloud cover (+)	90	17	86	20	49	11	80	13	77	9
OLR (-)	Omega 500 hPa (-)	82	20	77	22	75	22	75	15	76	10
Cloud cover (+)	Omega 500 hPa (-)	82	20	79	22	76	22	75	15	74	10
Cloud cover (+)	U wind 500 hPa (+)	82	18	76	20	68	18	46	10	48	7
OLR (-)	U wind 500 hPa (+)	81	18	73	21	64	19	46	12	44	7
U wind 500 hPa (+)	Omega 500 hPa (-)	75	19	69	21	61	20	47	11	44	7
Omega 500 hPa (-)	Div. 1000 hPa (-)	67	19	66	20	67	20	69	13	71	9
Div. 1000 hPa (-)	U wind 500 hPa (+)	63	17	63	19	56	17	46	10	44	7
Omega 500 hPa (-)	Vort. 1000 hPa (-)	63	16	54	16	55	16	64	12	67	9
Vort. 1000 hPa (-)	U wind 500 hPa (+)	59	16	51	17	42	16	44	9	38	6
V wind 500 hPa (-)	U wind 500 hPa (+)	58	15	53	17	51	17	45	10	45	7
Div. 1000 hPa (-)	Vort. 1000 hPa (-)	55	15	52	17	53	16	65	11	68	7

high in all study areas (up to 90 % in area A), as expected, except for study area C, where only 49 % of the days with SACZ episodes showed this intersection. On the other hand, the chance of having a SACZ episode given all the days when this intersection occurred (question *b*) was never higher than 20 %, as in study area B, and as low as 9 % in study area E, for example. This is explained by the influence of other meteorological systems, such as recurrent cold fronts, that cause a similar response in these two variables. The higher probabilities for question *b* were achieved combining omega at 500 hPa with OLR and cloud cover, when up to 22 % of the episodes would have been identified by their signature anomalous signals only in regions B and C. These results also varied considerably among the study areas. In addition, probabilities for question *b* were always lower than for question *a*, indicating that the combinations of the variables would often occur also in other conditions than the configuration of the SACZ or that the combinations of the given variables in SACZ days have more robust or well-determined behaviors.

After analyzing variables in pairs, several numbers of combinations were further experimented, until all five variables (with their corresponding signature anomalous signal) were intersected: negative OLR, negative omega at 500 hPa, negative vorticity at 1000 hPa, positive zonal component of wind (*u*) at 500 hPa and negative anomalies of horizontal wind divergence at 1000 hPa. This full intersection set achieved the greatest results for question *b*, as given in Table 5: 28 % of all SACZ days in regions A and B could be determined by the numerical assessment of the combined anomalies only, for example. On the other hand, 45 and 37 % of all days that presented the combination of the signature anomalies, occurred together with the convergence zone in regions A and B, respectively (question *a*).

Besides the 5 variables chosen, a temporal condition was added, in order to better characterize the SACZ: each variable should present its signature anomalous signal for at least 3 consecutive days, which made the intersection set even smaller. This analysis shifted the results of questions *a* and *b*: up to 46 % of all episodes of SACZ could be determined by the assessment of the selected variables, combined with the 3-day minimum persistence of their anomalous signals, in study area A, while only 19 % of all days that showed this combined set of characteristics had the SACZ configured. After considering this temporal condition, the probabilities of question *b* in all areas were greater than those of question *a*, pointing that however, this “full intersection” (anomalous signals + time condition) may not be very common among all SACZ days (10 % in area B, for example), almost half of them (46 % and 45 % in areas A and B, respectively) occur simultaneously with the SACZ, as given in Table 5. These percentages gradually decreased through other study areas, while moving southward, up to only 13 and 4 % in study area E (questions *a* and *b*, respectively). However, in individual analysis, a comparison between results

Table 5 Conditional probabilities combining all five selected variables: (a) $P(\text{full intersection}|\text{SACZ})$ and (b) $P(\text{SACZ}|\text{full intersection})$, comparing results with and without the 3-day minimum persistence condition of the anomalous signal in the full intersection set, per study area

	A		B		C		D		E	
	<i>a</i> (%)	<i>b</i> (%)								
1 day	45	28	37	28	32	24	34	15	30	9
≥3 days	19	46	10	45	6	34	6	25	4	13

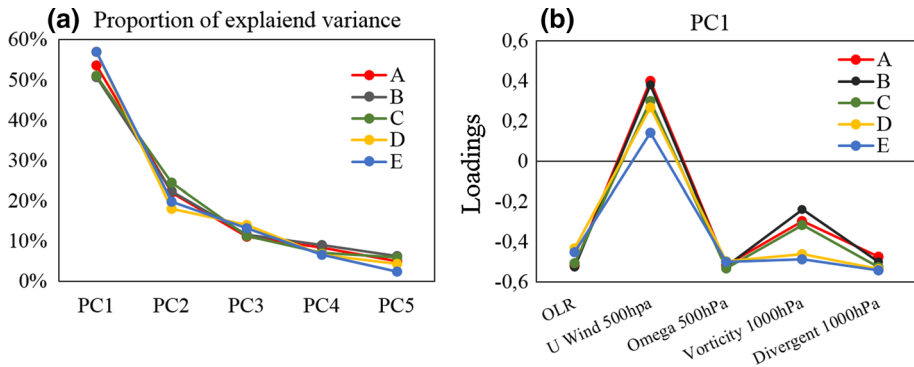


Fig. 5 **a** Proportion of variance of the group of chosen variables explained by each principal component. **b** Loadings of PC1 for each study area

before and after the addition of the 3-day condition shows that the persistence of the phenomenon plays an important role for its proper statistical characterization.

2.4 The making of the indices

Principal component analysis (PCA) was performed using sets of normalized anomalies of the entire daily series of the five chosen variables. The five study areas presented similar modes of variability, with their first principal components (PC1) explaining about 55 % of the variance of the group, dropping to 21 % of attribution to the second principal components (PC2) on average, as shown in Fig. 5a. The signals of the chosen variables displayed in the loadings of PC1 match with the SACZ-predominant anomalous signals, indicating its relationship with the main mode of variability of the set of variables, as shown in Fig. 5b. The magnitude of the loadings of PC1 also varied among the study areas: a gradient is observed with the zonal component of wind and the horizontal wind vorticity at 1000 hPa, in which the oceanic regions D and E showed significantly greater values when compared with the continental regions (Fig. 5b). The loadings of PC1 were then taken as coefficients of linear functions, multiplied by their associated original variables, to compose the local indices, such as exemplified in Eq. 1.

$$i_A = -0.516x_1 + 0.399x_2 - 0.513x_3 - 0.295x_4 - 0.471x_5 \tag{1}$$

where x_1, x_2, x_3, x_4 and x_5 represent the daily anomalies of OLR, zonal component of wind at 500 hPa, omega at 500 hPa, horizontal wind vorticity and divergence at 1000 hPa averaged over study area A, for example. This method generates similar results to the factors of PC1 directly. However, this approach allows an operational usage of the index, analyzing days as individuals for predicting SAMS behaviors, when long series are not available, as suggested by Silva and Carvalho (2007). All series of anomalies were first normalized between 0 and 1, with respect to their variation between January 2000 and June 2014, before applying the formula.

The relationship between the developed indices and the SAMS and its influence on precipitation was assessed with daily 0.5° resolution precipitation data, obtained from the CPC US Unified gauge-based precipitation analysis provided by NOAA/OAR/ESRL PSD

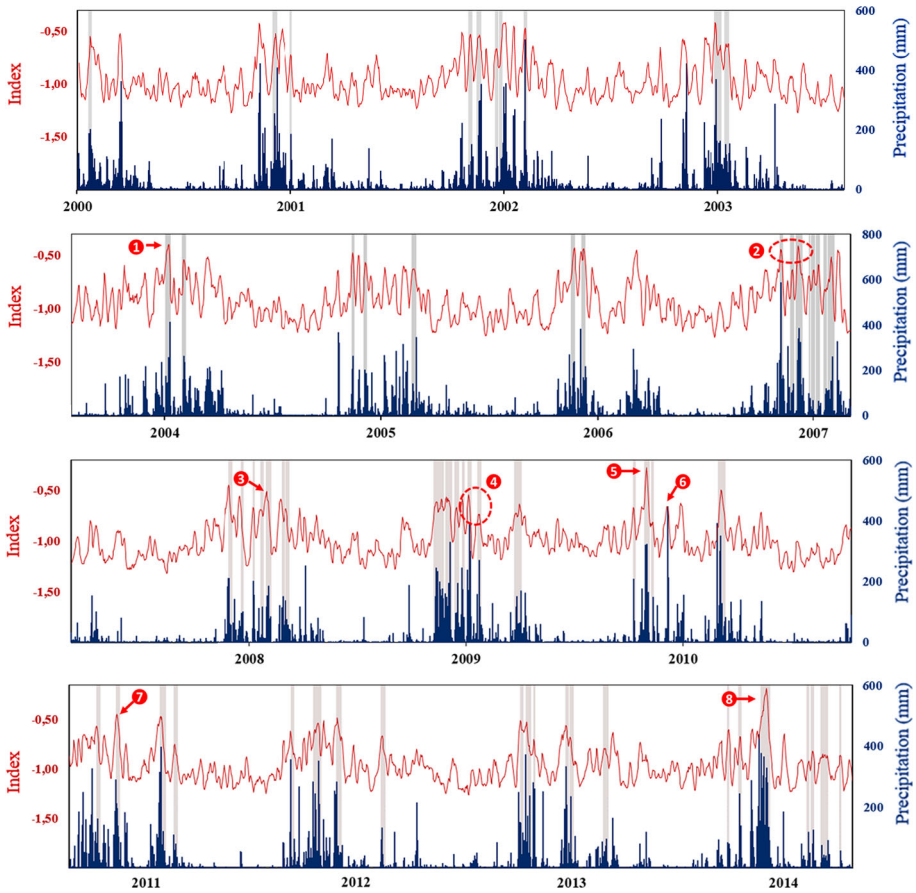


Fig. 6 Daily precipitation from CPC in blue bars, SACZ days in gray shading and the calculated index in red with a 5-day moving average. These series refer to study area A. Numbers indicate episodes with relevant impact to local communities, as detailed in Table 6

Table 6 Details of some extreme episodes and their impacts, as indicated with numbers in Fig. 7

Location	Deaths	Homeless (estimated)
1. Juiz de Fora, Caratinga and surroundings	6	900
2. Several towns—East of Minas Gerais	11	2000
3. Coroaç and surroundings	2	
4. Zona da Mata Mineira		7000
5. Carlos Chagas		300
6. Cachoeiro de Itapemirim		3000
7. Ubá, Visconde de Rio Branco and surroundings		500
8. Several towns—East of Minas Gerais and Espírito Santo	23	61,000

Data collected from Globo (2004, 2006, 2008, 2009, 2010, 2013) and Folha de São Paulo (2004, 2013) news agencies from their online versions

(Xie et al. 2010) averaged over the continental study areas A, B and C. For oceanic regions D and E, precipitation data from Reanalysis 2 (Kalnay et al. 1996) from NCEP were used.

3 Results and discussion

The indices presented a clear seasonal behavior, in accordance with the typical precipitation pattern of the regions, determined by the SAMS, which is stated by the correlation coefficients between indices and precipitation series: $r = 0.633, 0.526, 0.505, 0.594$ and 0.660 for study areas A, B, C, D and E, respectively. A positive correlation was also observed between the series of SACZ episodes and precipitation, with a coefficient $r = 0.451$ in study area A, gradually and latitudinally dropping to $r = 0.198$ in study area E. The disparity observed in the strength of these two analyses for region E demonstrates its local index best fit to the whole precipitation series, although the index obtained for region A closely follows both high-positive precipitation rates and SACZ occurrences, as shown in Fig. 6. In this graph, some examples of relevant extreme events of rainfall and floods occurred in the study areas and surroundings, with significant social impacts, are identified with numbers. Even though not all listed episodes occurred in study area A, due to proximity and strength of anomalies, their signal is noticed in this area as well. Details of these episodes are shown in Table 6 and their geographical location within the study areas is displayed in Fig. 7. This sample of events indicates the ability of the index to identify hazardous episodes that follow intense rainfall events on a daily basis.

In order to define a best index value to identify the SACZ, the indices' ranges of variation were equally divided in 21 quantiles and, for each limit value between quantiles (hereafter referred to as alpha— α , assuming values from 1 to 20), two probabilities were calculated: (1) days with SACZ episodes correctly identified, given the number of days with SACZ episodes and (2) days with SACZ episodes mistakenly identified (false alarms), given the number of days in which the SACZ did not occur. In both denominators of these two ratios, only days contained in the period from October to April were considered, suggested as the average months of onset and demise of the SAMS (Silva and Carvalho 2007; Gan et al. 2005). Taking these two probabilities and varying the quantiles (α), optimum identifying limits were obtained maximizing the result of the subtraction of the number of false alarms from the correctly identified episodes. In region A, the maximum difference was found taking the limit between the 13th and the 14th quantiles ($\alpha = 14$), where 47 days with episodes of SACZ were correctly identified (12 % of the 397 SACZ days), while 27 false alarms were accused (nearly 1 % of the 2695 days without SACZ episodes). This yielded the maximum 20-day difference (47 correct identifications—27 false alarms). Yet a second strategy was approached to define a less conservative best value for the index. Instead of maximizing this subtraction expressed in number of days, the difference was optimized in percentages, proportionally, considering the amount of days the SACZ occurred and the remaining days, when it did not occur. This approach yielded different results, once these two groups vary significantly in size. We subtracted the ratios of correctly identified SACZ days, given the total number of SACZ days, from the false alarms, given the number of days when the SACZ did not occur: $P(\text{correct SACZ days} / \text{total SACZ days}) - P(\text{false alarm SACZ days} / \text{total non-SACZ days})$. For study area A, considering these proportions, the index value between the 7th and the 8th quantiles ($\alpha = 8$) was found to be the best, where 89 % of all SACZ days were correctly identified (355 out of the 397 days), while its configuration was mistakenly pointed in 32 % of all non-SACZ

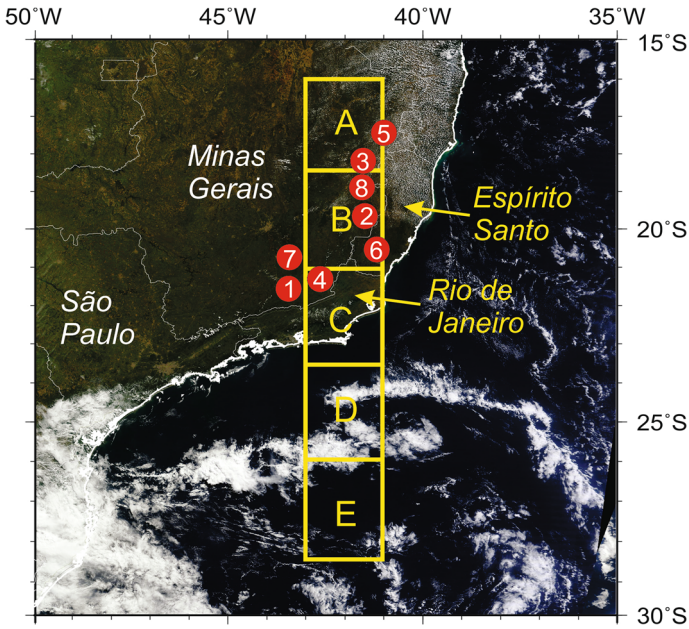


Fig. 7 Location of the episodes identified in Table 6 within the study areas in Southeast Brazil

days (882 out of 2695), reaching the maximum 57 % proportional difference. These two optimization strategies are illustrated in Fig. 8.

The indices were also tested to identify days with positive extreme precipitation events during the active phase of the SAMS (October–April). Extreme precipitation events were defined as the 20 % days with the greatest precipitation accumulated daily values per study area. In study area A, for example, the best absolute difference was obtained when the index correctly identified 663 days of extreme precipitation during the wet period (68 % of the 978 days) and mistakenly identified 256 days without extreme precipitation values

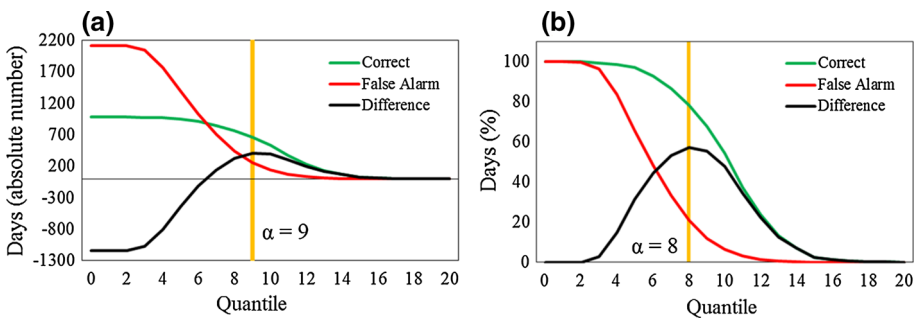


Fig. 8 **a** Correctly identified SACZ days (green line), false alarms (red line) and the difference between these two (black line), varying with the index obtained for region A. The maximum difference is highlighted with a yellow bar, indicating the corresponding limit between quantiles (α). **b** Same as in **a**, but in terms of proportions: correctly identified SACZ, given the number of SACZ days, and false alarms, given the number of non-SACZ days

Table 7 (a) Best index quantiles (α) and associated correctly identified days with SACZ and false alarms, considering the maximum absolute and proportional differences, (b) same as in (a), but for the identification of extreme rainfall during the SAMS active phase (October–April)

	A			B			C			D			E		
	Correct (%)	False alarm (%)	α	Correct (%)	False alarm (%)	α	Correct (%)	False alarm (%)	α	Correct (%)	False alarm (%)	α	Correct (%)	False alarm (%)	α
(a) Days with SACZ episodes															
Max. abs. difference	12	1	14	12	1	14	4	1	15	0.3	0.1	18	2	0.1	17
Max. proportional difference	89	32	8	79	27	9	84	40	8	77	33	9	81	48	8
(b) Days of extreme rainfall, during SAMS months															
Max. abs. difference	68	32	9	79	27	10	84	40	10	77	33	11	81	48	10
Max. proportional difference	78	21	8	72	18	9	86	31	8	81	22	9	79	15	9

(12 % of the 2114 days where precipitation was not positively extreme during the wet period), taking $\alpha = 9$. The best proportional difference was obtained when 78 % of the extreme precipitation days in the period were correctly identified (767 out of 978 days), while 21 % of the days in this period of non-extreme precipitation were pointed as so (443 out of 256 days), with $\alpha = 8$. A summary of the results of these two tests, for all five study areas, is presented in Table 7.

For the SACZ identification, the index showed itself to be more reliable in study areas A and B, where the correct attribution of 12 % of all SACZ days implied on only nearly 1 % false alarms of the non-SACZ days. The values of the indices defined by the greatest proportional differences achieved similar results throughout the five study areas. In study area C, for instance, the correct identification of 84 % of all SACZ days implied a false-alarm rate of 40 % of all non-SACZ days, even though this represents considerably more incorrect attributions (1047 days) than correct ones (419 days).

Better results were achieved when identifying extreme precipitation days during the SAMS active phase, when all tests presented, in both strategies, more accuracies than false alarms. A considerable difference was observed in region D, for example, where only 165 days were mistakenly identified as extremes of precipitation (which is equivalent to 7 % of the 2268 non-extreme precipitation days), while 443 days of extreme precipitation were correctly identified by the index (54 % of the 824 days of extreme precipitation). With this second analysis, on average, a 61.6 % accuracy yielded a 9.6 % false-alarm probability, achieved with the maximization of the absolute difference approach. Taking the proportional difference strategy, on average, a 79.2 % accuracy yielded a 21.4 % false-alarm rate.

In addition, the identification of extreme rainfall episodes during the wet period pointed to best α -values closer to the mean ($8 \leq \alpha \leq 11$), while the identification of the SACZ yielded higher best α -values, especially when considering the absolute difference strategy ($14 \leq \alpha \leq 18$), which indicates the very extreme character of precipitation volumes associated with this phenomenon.

4 Conclusion

The influence of the SACZ on atmospheric variables was assessed for the period between January 2000 and June 2014, even though some of the chosen variables have already been traditionally used as identifiers for the phenomenon, such as OLR anomalies, for example, but never before with such a quantitative approach, as we are concerned. A primary probability analysis pointed that up to around 46 % of all SACZ episodes could be identified only by a local numerical assessment of the variables where its signature is clearly observed: zonal component of wind and vertical velocity (omega) at 500 hPa, horizontal wind vorticity and divergence at 1000 hPa and OLR. These variables, here referred to as “signature variables,” presented consistent predominant anomalous signals associated with the SACZ in the five considered study areas.

The developed indices were more efficient in identifying SACZ episodes in the northernmost study areas, where its influence on the variables was more clear, reaching simultaneous 12 % accuracy and 1 % false-alarm rates. This is explained by the weaker influence of cold fronts, which cause similar signals in the selected variables, but do not often reach very low latitudes. A better result was achieved with the identification of extreme precipitation events only in the period from October to April, which comprehends the region’s wet season, determined by active phase of the SAMS, when the number of accurate results was

always greater than false alarms, with considerably big differences in all tests performed. Averaging the results of the five studied regions, a 61.6 % accuracy yielded a 9.6 % false-alarm probability, achieved with the maximization of the absolute difference approach, and a 79.2 % accuracy yielded a 21.4 % false-alarm rate, with the proportional difference strategy.

In addition, the local-scale approach showed that different variables can be used to compose different indices for separate regions affected by the monsoon, even reproducing this same methodology. This way, local indices may be determined to other areas, considering local specificities and, thus, better adapting to small-scale needs for predicting hazardous episodes. For example, negative anomalies of the meridional component of wind seemed to be associated with the SACZ in the southernmost study areas. This ability of small-scale indices may be lost if the SAMS is studied in its continental scale.

The presented indices are reliable alternatives for the identification of extreme precipitation anomalies associated with the SAMS from various sources of data, when observed rainfall is not available or its resolution is too coarse, which is often the case of observed precipitation series. Additionally, the variables that compose the indices are common outputs of weather and climate models, as well as the usage of PCA by the scientific community, which makes the suggested methodology easily reproducible and extensible to other periods. Therefore, the indices may serve as operational public management tools for the assessment and prediction of local extreme precipitation conditions in the regions affected by the SAMS, helping prepare for its impacts on society.

Acknowledgments We are thankful to Raquel Brisson, Beatriz Malta and Ana Roland for their support, to Fundação Carlos Chagas Filho de Amparo à Pesquisa do Rio de Janeiro (FAPERJ) for providing financial aid and to the reviewers for their valuable contributions.

References

- Ahern M, Kovats RS, Wilkinson P, Few R, Matthies F (2005) Global health impacts of floods: epidemiologic evidence. *Epidemiol Rev* 27:36–46. doi:[10.1093/epirev/mxi004](https://doi.org/10.1093/epirev/mxi004)
- Ambrizzi T, Ferraz SE (2015) An objective criterion for determining the South Atlantic Convergence Zone. *Front Environ Sci* 3:23
- Andrade FM, Marton E (2008) Caracterização espacial dos eventos de ZCAS nos verões de 2005/2006 e 2006/2007. In: XV Congresso Brasileiro de Meteorologia, São Paulo, SP. Anais do XV Congresso Brasileiro de Meteorologia. SBMET
- Avelar AS, Netto AL, Lacerda WA, Becker LB, Mendonça MB (2013) Mechanisms of the recent catastrophic landslides in the mountainous range of Rio de Janeiro, Brazil. In: *Landslide science and practice*. Springer, Berlin, pp 265–270. doi:[10.1007/978-3-642-31337-0_34](https://doi.org/10.1007/978-3-642-31337-0_34)
- Barbosa HA, Kumar TL, Silva LRM (2015) Recent trends in vegetation dynamics in the South America and their relationship to rainfall. *Nat Hazards* 77(2):883–899
- Bluestein HB (1992) Synoptic-dynamic meteorology in midlatitudes. *Principles of kinematics and dynamics*, vol 1. Oxford University Press, Oxford
- Carvalho LM, Jones C, Liebmann B (2002) Extreme precipitation events in southeastern South America and large-scale convective patterns in the South Atlantic convergence zone. *J Clim* 15(17):2377–2394
- Carvalho LM, Jones C, Liebmann B (2004) The South Atlantic convergence zone: intensity, form, persistence, and relationships with intraseasonal to interannual activity and extreme rainfall. *J Clim* 17(1):88–108
- Carvalho LM, Silva AE, Jones C, Liebmann B, Dias PLS, Rocha HR (2011) Moisture transport and intraseasonal variability in the South America monsoon system. *Clim Dyn* 36(9–10):1865–1880
- Climanálise (2011) Boletim de Monitoramento e Análise Climática, vol 26, no 1. Centro de Previsão do Tempo e Estudos Climáticos and Instituto Nacional de Pesquisas Espaciais (CPTEC/INPE), Brazil. <http://climanalise.cptec.inpe.br/~rclimanl/boletim/pdf/pdf11/jan11.pdf>. Accessed July 2015

- Climanálise (2000–2014) Boletim de Monitoramento e Análise Climática, vol 15–26, no 1–6. Centro de Previsão do Tempo e Estudos Climáticos and Instituto Nacional de Pesquisas Espaciais (CPTEC/INPE), Brazil. <http://goo.gl/DzZ5fL>. Accessed July 2015
- Coelho CA, Cardoso DH, Firpo MA (2015a) Precipitation diagnostics of an exceptionally dry event in São Paulo Brazil. *Theor Appl Climatol*. doi:10.1007/s00704-015-1540-9
- Coelho CA, de Oliveira CP, Ambrizzi T, Reboita MS, Carpenedo CB, Campos JLPS, Rehbein A (2015b) The 2014 southeast Brazil austral summer drought: regional scale mechanisms and teleconnections. *Clim Dyn*. doi:10.007/s00382-015-2800-1
- Contador CS, Nielsen DM, Smiderle OSM, Cataldi M, da Hora MAGM (2013) Avaliação da Influência da Umidade na Primavera da Região Amazônica na Ocorrência da ZCAS. In: V Simpósio Internacional de Climatologia, 2013, Florianópolis. Anais do V Simpósio Internacional de Climatologia
- Dourado F, Arraes TC and Silva M (2012) O Megadesastre da Região Serrana do Rio de Janeiro: as causas do evento, os mecanismos dos movimentos de massa e a distribuição espacial dos investimentos de reconstrução no pós-desastre. *Anuário do Instituto de Geociências*, 35(2):43–54. ISSN 0101-9759. doi:10.11137/2012_2_43_54
- Drumond ARM, Ambrizzi T (2005) The role of SST on the South American atmospheric circulation during January, February and March 2001. *Clim Dyn* 24(7–8):781–791
- Ferreira NJ, Sanches M, Silva Dias MAF (2004) Composição da zona de convergência do Atlântico Sul em períodos de El Niño e La Niña. *Rev Bras Meteorol* 19(1):89–98
- Folha de São Paulo (2004) Chega a nove o número de mortos em Minas por causa das chuvas. *Cotidiano*. <http://goo.gl/0V3WPx>. Accessed 22 Nov 2015
- Folha de São Paulo (2013) Espírito Santo enfrenta a maior chuva da história, afirma governo. *Cotidiano*. <http://goo.gl/UsHL2B>. Accessed 22 Nov 2015
- Gan MA, Rao VB, Moscat MC (2005) South American monsoon indices. *Atmos Sci Lett* 6(4):219–223
- Globo (2004) Em Minas, 14 mortes. *Bom dia Brasil*. goo.gl/G33LeL. Accessed 22 Nov 2015
- Globo (2006) Moradores do leste de MG sofrem com estragos causados pelas fortes chuvas. *Bom dia Brasil*. <http://goo.gl/jqWaVS>. Accessed 22 Nov 2015
- Globo (2008) Dramas do verão chuvoso. *Bom dia Brasil*. <http://goo.gl/1tx5ts>. Accessed 22 Nov 2015
- Globo (2009) Chuva não dá trégua para interior de Minas Gerais. *Bom dia Brasil*. <http://goo.gl/c4EtRk>. Accessed 22 Nov 2015
- Globo (2010) Bombeiros retomam buscas por desaparecida após enchente, em MG. Minas Gerais. <http://goo.gl/5AzSXn>. Accessed 22 Nov 2015
- Globo (2013) Defesa Civil contabiliza 23 mortes em decorrência da chuva no ES. Espírito Santo. <http://goo.gl/x0CFH5>. Accessed 22 Nov 2015
- Güneralp B, Güneralp İ, Liu Y (2015) Changing global patterns of urban exposure to flood and drought hazards. *Glob Environ Change* 31:217–225. doi:10.1016/j.gloenvcha.2015.01.002
- Jones C, Carvalho LM (2001) Active and break phases in the South American monsoon system. *J Clim* 15:905–914
- Kalnay EM, Kanamitsu R, Kistler W, Collins D, Deaven L, Gandin M, Iredell S, Saha G, White J, Woollen Y, Zhu M, Chelliah W, Ebisuzaki W, Higgins J, Janowiak KC, Mo C, Ropelewski J, Wang A, Leetmaa R, Reynolds R, Jenne R, Joseph D (1996) The NCEP/NCAR 40-year reanalysis project. *Bull Am Meteorol Soc* 77(3):437–471
- Kousky VE (1988) Pentad outgoing longwave radiation climatology for the South American sector. *Rev Bras Meteorol* 3(1):217–231
- Kousky VE, Gan MA (1981) Upper tropospheric cyclonic vortices in the tropical South Atlantic. *Tellus* 33:538–551. doi:10.1111/j.2153-3490.1981.tb01780.x
- Lejeune Q, Davin EL, Guillod BP, Seneviratne SI (2015) Influence of Amazonian deforestation on the future evolution of regional surface fluxes, circulation, surface temperature and precipitation. *Clim Dyn* 44(9–10):2769–2786. doi:10.1007/s00382-014-2203-8
- Lenters JD, Cook KH (1997) On the origin of the Bolivian high and related circulation features of the South American climate. *J Atmos Sci* 54(5):656–678. doi:10.1175/1520-0469(1997)054<0656:OTOOTB>2.0.CO;2
- Lima KC, Satyamurty P, Fernández JPR (2010) Large-scale atmospheric conditions associated with heavy rainfall episodes in Southeast Brazil. *Theor Appl Climatol* 101(1–2):121–135. doi:10.1007/s00704-009-0207-9
- Mendonça RWB, Bonatti JP (2008) Estudo da energética modal para episódios de ZCAS. Parte I: análise observacional. *Rev Bras Meteorol* 23(4):360–380. doi:10.1590/S0102-77862008000400001
- Milly PCD, Wetherald RT, Dunne KA, Delworth TL (2002) Increasing risk of great floods in a changing climate. *Nature* 415(6871):514–517. doi:10.1038/415514a

- Minuzzi RB, Sediyaama GC, Barbosa EDM, Melo Júnior JCFD (2007) Climatologia do comportamento do período chuvoso da região sudeste do Brasil. *Rev Bras Meteorol* 22(3):338–344
- Murphy SJ, Washington R, Downing TE, Martin RV, Ziervogel G, Preston A, Todd M, Butterfield R, Briden J (2001) Seasonal forecasting for climate hazards: prospects and responses. *Nat Hazards* 23(2–3):171–196. doi:[10.1023/A:1011160904414](https://doi.org/10.1023/A:1011160904414)
- Neto OBS, Escobar G, Silva P (2010) Método objetivo para identificar episódios de Zonas de Convergência de Umidade (ZCOU) no ambiente operacional do Centro de Previsão de Tempo e Estados Climáticos-CPTEC. In: Congresso Brasileiro De Meteorologia, vol 16, Belém do Pará, Brazil
- Nicolini M, Saulo C, Ulke G, Marengo J, Douglas M, Paegle J, Zipser E (2004) South American low-level jet diurnal cycle and three-dimensional structure. *CLIVAR Exchanges*, vol 9, no 1, International CLIVAR Project Office, pp 6–9
- ONS (Operador Nacional do Sistema Elétrico) (2013) Dados relevantes. <http://goo.gl/b8tC7Q>. Accessed 05 July 2015
- Prohaska F (1976) Climates of Central and South America. In: Schwerdtfeger W (ed) *World survey of climatology*. Elsevier, Amsterdam, pp 13–72
- Quadro MFL (1999) Estudo de episódios de zonas de convergência do Atlântico Sul (ZCAS) sobre a América do Sul. *Rev Bras Geofís (Print Version)* 17:210, 199
- Saraiva GSZ, dos Santos EV, Coelho JOM, Egas HM, Casagrande L (2015) A Atuação da ZCAS no Desastre de Dezembro de 2013 no Sudeste do Brasil. In: Workshop ZCAS/Monção. July 2015. CPTEC/INPE—Cachoeira Paulista, São Paulo, Brazil. <http://goo.gl/eD6Tt8>. Accessed July 2015
- Seluchi ME, Chou SC (2009) Synoptic patterns associated with landslide events in the Serra do Mar. *Braz Theor Appl Climatol* 98(1):67–77. doi:[10.1007/s00704-008-0101-x](https://doi.org/10.1007/s00704-008-0101-x)
- Siegel FR (2014) Shelter: proactive planning to protect citizens from natural hazards. In: *Countering 21st century social-environmental threats to growing global populations*. Springer, pp 53–67. doi:[10.1007/978-3-319-09686-5_4](https://doi.org/10.1007/978-3-319-09686-5_4)
- Silva AE, Carvalho LMV (2007) Large-scale index for South America Monsoon (LISAM). *Atmos Sci Lett* 8(2):51–57. doi:[10.1002/asl.150](https://doi.org/10.1002/asl.150)
- Silva Dias PL, Schubert WH, DeMaria M (1983) Large-scale response of the tropical atmosphere to transient convection. *J Atmos Sci* 40(11):2689–2707
- Singh O, Kumar M (2013) Flood events, fatalities and damages in India from 1978 to 2006. *Nat Hazards* 69(3):1815–1834. doi:[10.1007/s11069-013-0781-0](https://doi.org/10.1007/s11069-013-0781-0)
- Spokane AR, Mori Y, Martinez F (2013) Housing arrays following disasters social vulnerability considerations in designing transitional communities. *Environ Behav* 45(7):887–911. doi:[10.1177/0013916512447799](https://doi.org/10.1177/0013916512447799)
- Stensrud DJ (1996) Importance of low-level jet to climate: a review. *J Clim* 9(8):1689–1711
- van der Ent RJ, Savenije HHG, Schaeffli B, Steele-Dunne SC (2010) Origin and fate of atmospheric moisture over continents. *Water Resour Res*. doi:[10.1029/2010WR009127](https://doi.org/10.1029/2010WR009127)
- Vera C, Higgins W, Amador J, Ambrizzi T, Garreaud R, Gochis D, Gutzler D, Lettenmaier D, Marengo J, Mechoso CR, Noguez Paegle J, Silva Dias PL, Zhang C (2006a) Toward a unified view of the American monsoon systems. *J Clim* 19(20):4977–5000
- Vera C, Baez J, Douglas M, Emmanuel CB, Marengo J, Meitin J, Nicolini M, Noguez-Paegle J, Paegle J, Penalba O, Salio P, Saulo C, Silva Dias MA, Silva Dias P, Zipser E (2006b) The South American low-level jet experiment. *Bull Am Meteorol Soc* 87:63–77
- World Meteorological Organization (2012) WMO statement of the status of the global climate in 2011. http://www.wmo.int/pages/prog/wcp/wcdmp/documents/1085_en.pdf. No. 1085. Switzerland. ISBN 978-92-63-11085-5. Accessed 27 Apr 2016
- Xie P, Chen M, Shi W (2010) CPC unified gauge-based analysis of global daily precipitation. In: *Preprints, 24th conference on hydrology*, Atlanta, GA, Am. Meteorol Soc, vol 2
- Zilli MT, Carvalho LV (2013) Frequency analysis of extreme events based on precipitation station data over southeastern Brazil. In: *AGU fall meeting abstracts*, vol 1, p 1361